Hybrid Positioning Aided Amorphous-Cell Assisted User-Centric Visible Light Downlink Techniques

Simeng Feng, Xuan Li, Rong Zhang, *Senior Member, IEEE,* Ming Jiang, *Senior Member, IEEE,*
Lajos Hanzo, *Fellow, IEEE*

***Abstract*—Visible Light Communications (VLC) has attracted significant attention in recent years, where the novel concept of User-Centric (UC) VLC based on Amorphous cells (A-Cells) exhibits extra benefits compared to conventional circular cells. The construction of A-Cells relies on the knowledge of the users' positions, hence the intrinsic amalgamation of VLC and positioning becomes important. Therefore we propose a novel hybrid positioning technique by beneficially combining the low-complexity of triangulation based positioning and the high accuracy of fingerprinting, in order to support A-Cell assisted UC VLC under practical LED linearity constraints with clipping distortion and noise. Our simulation results demonstrate that the proposed technique is capable of achieving a much higher positioning accuracy than triangulation at a lower complexity than fingerprinting, where the resultant system throughput is similar to that of perfect positioning.**

***Index Terms*—Amorphous cell, indoor positioning technique, visible light communication.**

I. Introduction

TO meet the escalating tele-traffic demand of a vibrant society and to sustain healthy economical growth, mobile networks have resorted to multi-layered Heterogeneous Network (HetNet) architectures, whilst simultaneously conquering higher carrier frequency bands [1]. As a promising candidate component for the future 5G HetNet, Visible Light Communications (VLC) relying on Light Emitting Diodes (LEDs) as Access Points (AP) has attracted substantial attention from both academia and industry. VLC relies on modulating data onto the light intensity produced by LEDs at rates way above the human eye's fusion frequency and on detecting the optical signal intensities via direct detection using an inexpensive photo-detector. Tremendous efforts have been invested in improving the link-level performance between a single LED array and a single user [2], [3], [4], [5]. Furthermore at the time of writing the research efforts dedicated to VLC aided networks relying on multiple LED arrays for supporting multiple users are also intensifying [6], [7], [8], [9]. Hence the appropriate construction of VLC cells is of the utmost importance.

In the post-4G era, several innovative concepts have been proposed for cell construction, such as 'liquid' cells and 'soft' cells [10]. These ideas have inspired the conception of User-Centric (UC) cell-design for VLC. Compared to the family of conventional Network-Centric (NC) design, the UC VLC concept has a higher grade of flexibility, because the resultant cell boundary can be adjusted according to the users' positions, hence resulting in so-called Amorphous Cells (A-Cells) [11][12]. In order to construct A-Cells for UC VLC, the users' positions have to be determined, although in the prior art [11] the idealized simplifying assumption was stipulated that the user-positions were known. Hence, integrating the A-Cell construction with positioning becomes essential. In the literature of indoor positioning, several techniques relying for example on triangulation based positioning and scene analysis have been studied [13], [14], [15], [16], where the associated positioning accuracy depends on the scenario considered. Against this background, in this paper, *we propose a hybrid positioning technique for beneficially combining the low-complexity of triangulation based positioning and high-accuracy of scene analysis in order to design an A-Cell assisted UC VLC system under practical LED linearity constraints in the presence of both clipping distortion and noise*.

The rest of the paper is organised as follows. Firstly, the VLC channel model and the A-Cell construction are introduced in Section 2. This is followed by our discussions on traditional positioning techniques and on the proposed hybrid positioning technique of Section 3. Finally, our performance results are provided in Section 4 and we conclude in Section 5. Furthermore, in TABLE I we define the abbreviations and acronyms according to first time used in our paper.

II. System Model

Consider a room size of $15m \times 15m \times 3m$, where a total of $N = 8 \times 8 = 64$ APs are uniformly installed at a height $H = 2.5m$ from the floor and a total of $K = 20$ desktop users are randomly distributed at a desk-height of $h = 0.85m$ from the floor. Furthermore, each AP consists of an array of LEDs provided both for illumination and optical transmission [17], where the transmitted optical power of each AP is $P_{Tx,opt}$ = $20W$. We now briefly introduce the VLC channel model and the A-Cell construction philosophy.

A. Channel Model

According to [17], within the half of the user's Field-of-View (FOV) denoted by ψ_c, the Line-of-Sight (LOS) channel spanning from the nth AP to the kth user can be formulated as:

$$h^0_{k,n} = \frac{(m+1)A_r}{2\pi D_d^2} \cos^m(\phi) T_s(\psi) g(\psi) \cos(\psi), \qquad 0 \le \psi \le \psi_c, \tag{1}$$

The financial support of the EPSRC projects (EP/N004558/1 and EP/N023862/1) and that of the European Research Councils (ERC) Advanced Fellow Grant is gratefully acknowledged. The data from the paper can be obtained from the University of Southampton ePrints research repository: 10.5258/SOTON/393915.

TABLE I
ABBREVIATIONS AND THEIR FULL NAME

Abbreviation	Full Name
VLC	Visible Light Communications
UC	User Centric
A-Cells	Amorphous Cells
LED	Light Emitting Diodes
HetNet	Heterogeneous Network
AP	Access Point
NC	Network Centric
FOV	Field of View
LOS	Light of Sight
CA	Coverage Area
FWHM	Full Width at Half Maximum
IAI	Inter-AP Interference
SINR	Signal to Interference plus Noise Radio
ZF	Zero Forcing
VT	Vectorized Transmission
OFDM	Orthogonal Frequency Division Multiplexing
ACO-OFDM	Asymmetrically Clipped Optical OFDM
F-Cells	Fixed Cells
O/E	Optical to Electrical
DC	Direct Current
RSS	Received Signal Strength
ML	Maximum Likelihood

where m is the order of Lambertian emission, which can be calculated by $m = \ln(2)/\ln[\cos(\phi_{1/2})]$, and $\phi_{1/2}$ denotes the semi-angle at half power. Furthermore, D_d is the distance between the nth AP and the kth user, ϕ is the angle of irradiance, ψ is the angle of incidence. Finally, $T_s(\psi)$ is the gain of the optical filter and $g(\psi)$ is the gain of the optical concentrator, which is non-zero for $0 \leq \psi \leq \psi_c$ and it is given by $g(\psi) = n^2/\sin^2(\psi_c)$.

In addition to the LOS path, the light will travel through many reflections, but we only consider the most significant first reflection caused by the walls, since they are the most dominant ones [11]. In this case, the total reflections between the nth AP and the kth user is given by: $h^1_{k,n} = \int_{walls} dh^1_{k,n}$, where $dh^1_{k,n}$ represents the reflection term owing to a small reflection point. Within the half of the user's FOV ψ_c, we have:

$$\begin{aligned} dh^1_{k,n} =& \frac{(m+1)A_r}{2\pi^2 D_1^2 D_2^2}\rho dA_{wall}\cos^m(\phi)\cos(\alpha)\cos(\beta) \\ & T_s(\psi)g(\psi)\cos(\psi), \qquad 0 \leq \psi \leq \psi_c, \end{aligned} \tag{2}$$

where D_1 is the distance between the nth AP and the reflection point, while D_2 is the distance between the reflection point and the kth user. Furthermore, ρ is the reflection efficiency of the surface, dA_{wall} is the reflective area, α and β are the angle of irradiance to the reflection point and to the user, respectively.

B. Amorphous Cell Construction

Conventional NC design of the VLC cells does not take into account the users' positions. This is inefficient, since the users in indoor VLC systems are usually sporadic. Moreover, in indoor VLC systems, the number of APs may be higher than the number of users, hence creating a dense AP deployment scenario. Therefore, we propose A-Cells from a user-centric point of view by considering the users' positions estimated by a positioning technique, where we introduce the *radius based A-Cell* construction method as follows.

Let us first introduce some common notations. We let $\mathcal{C}$ be the specific set hosting all cells, where for the cth cell $\mathcal{C}_c$, we have $|\mathcal{N}_c|$ APs hosted in the set $\mathcal{N}_c$ serving $|\mathcal{K}_c|$ users of the set $\mathcal{K}_c$, with $|\cdot|$ being the cardinality of a set. We firstly construct a full user-to-network association matrix $\boldsymbol{M}^f$ having K rows and N columns corresponding to K users and N APs. The $[k,n]$th entry of $\boldsymbol{M}^f$ is set to as $h^0_{k,n} + h^1_{k,n}$. We then carry out AP anchoring as follows:

1) Initialise the user-to-network association matrix $\boldsymbol{M} = \boldsymbol{M}^f$.
2) Find the best user-AP pair $[k^*, n^*]$ having the highest channel quality amongst all the entries of $\boldsymbol{M}$ and then collect the best user-index k^* in $\boldsymbol{k}^*$ and AP-index n^* in $\boldsymbol{n}^*$.
3) Set all entries in the k^*th row and in the n^*th column of $\boldsymbol{M}$ to zero in order to exclude them from further consideration throughout the AP anchoring process.
4) If there are still positive entries in $\boldsymbol{M}$, we repeat this process from Step 2 onwards. Otherwise, we output $\boldsymbol{M}$ as the sub-matrix of $\boldsymbol{M}^f$ constituted by all rows from $\boldsymbol{k}^*$ and set $\boldsymbol{M}$ to zero excluding the [$\boldsymbol{k}^*$, $\boldsymbol{n}^*$] entries.

The objective of AP anchoring is to have exclusive user-AP pairs for ensuring that each of those users in $\boldsymbol{k}^*$ will be served by its own anchor AP.

Having generated the user-to-network association matrix $\boldsymbol{M}$, the *radius based A-Cells* can be constructed, where the users are firstly grouped based on a pre-defined distance threshold d_0 and then we select APs associated with those users as follows:

1) Initialise cell $\mathcal{C}_c = \{\emptyset\}$ and introduce the counter c, which is initialised as $c = 1$.
2) We commence by forming cell $\mathcal{C}_c$ upon recruiting the first user, who is selected randomly and has not been included in any cells. Hence, this user will be the only one in the set $\mathcal{K}_c$, who will be supported by the associated AP set $\mathcal{N}_c$ containing the AP associated with this user according to the matrix $\boldsymbol{M}$.
3) Recruit another user(s) from the set of hitherto unassigned users, who has a distance shorter than d_0 from the first user in cell $\mathcal{C}_c$. Then update the cell $\mathcal{C}_c$, which results in the expanded set of $\mathcal{K}_c$ and $\mathcal{N}_c$.
4) Set all entries of the association matrix $\boldsymbol{M}$ supporting the users in $\mathcal{K}_c$ to zero. If there are still positive entries in $\boldsymbol{M}$, we increase c and repeat the Step 3 and Step 4.

Figure 1(a) illustrates the conventional NC design serving 20 users (marked by circles), whose positions are generated from a uniform random distribution. The NC design divides the room into four square cells and within each cell, there are (4×4) 16 APs (marked by triangles). The problem this design has to solve is that of *unbalanced loading*, where the bottom-left cell has a significantly lower user-load than the rest of

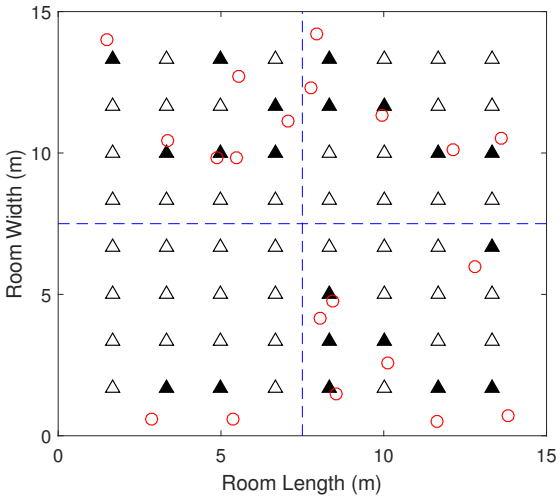

(a) Network-Centric Design with Fixed Cell Boundary

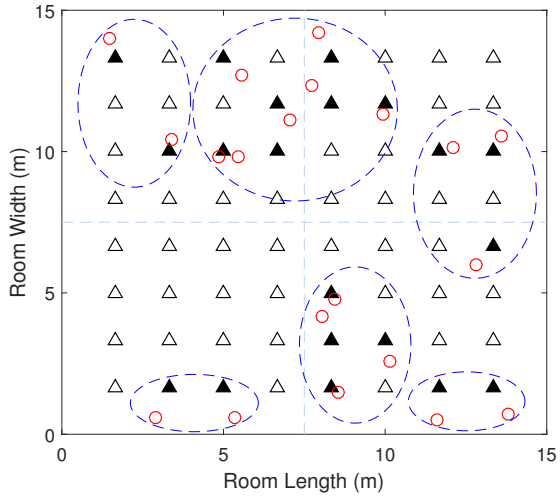

(b) Amorphous-Cells with Flexible Cell Boundary

Fig. 1. Illustration of the conventional and of the amorphous cells. (a) Fixed cells (F-Cells) shown in dashed line with 8 × 8 = 64 APs represented by triangles serving 20 users marked by circles, where the associated APs after anchoring are marked by solid triangles. (b) displays the radius-based A-Cells shown in dash ellipses under the same scenario as (a).

the cells. However, the UC design portrayed in Figure 1(b) is capable of improving the limitation of the NC design.

C. System Measurement

In VLC, each AP has its own adequate coverage area (CA), which depends on the AP's semi-angle at half power (FWHM) and on the user's FOV. The Inter-AP Interference (IAI) is imposed at the overlapping area of two or more atto-cells, which may degrade the received Signal to Interference plus Noise Ratio (SINR). In order to mitigate the influence of IAI, we can associate multiple APs with multiple users to form A-cells according to Section 2.2 and employ Zero-Forcing (ZF)-based Vectorized Transmission (VT)[7]. In this way, interference will only occur amongst different A-cells, which is more benign, since the A-cells are naturally separated as a benefit of their users' position-aware construction. The signal transmitted within each A-cell using VT is then further modulated, employing Asymmetrically Clipped Optical OFDM (ACO-OFDM) for the link-level transmission. To elaborate a little further, ACO-OFDM relies on the Hermitian symmetry for generating real-valued and positive outputs. After applying ZF-based VT and ACO-OFDM for the A-cell $\mathcal{C}_c$, the SINR of a specific user $k \in \mathcal{K}_c$ may be written as:

$$\lambda_{c,k} = \frac{\gamma^2 \pi P_{Tx,opt}^2 \omega_c^2}{N_0 B + \gamma^2 \pi P_{Tx,opt}^2 \sum_{i \in S_I} (h_{i,k}^0 + h_{i,k}^1)^2}, \quad (3)$$

where we have

$$\omega_c = \min_{\mu=1,\ldots,|\mathcal{N}_c|} \sqrt{\frac{1}{||\boldsymbol{G}_c(\mu,:)||_F^2}}, \quad (4)$$

where $\boldsymbol{G}_c = \boldsymbol{H}_c^H (\boldsymbol{H}_c \boldsymbol{H}_c^H)^{-1}$ is the ZF pre-coding matrix employed in $\mathcal{C}_c$, with $\boldsymbol{H}_c$ being the channel matrix hosting all channels between the set $|\mathcal{N}_c|$ of APs and the $|\mathcal{K}_c|$ users in $\mathcal{C}_c$. Furthermore, γ is the O/E conversion efficiency, $N_0 \approx 10^{-22}$ A^2/Hz is the noise power spectral density and the bandwidth B is set to 20 MHz. Finally, S_I is interference set arriving from the APs involved in all the A-Cells, excluding $\mathcal{C}_c$.

Let us now consider a more practical situation by introducing clipping distortion and noise. Practical LEDs typically exhibit a limited linear range of $[I_{min}, I_{max}]$, which corresponds to the optical power range of $[P_{Tx,min}, P_{Tx,max}]$ [18]. Furthermore, according to the current-voltage characteristic of the LED, a DC bias with power $P_{Tx,bias}$ has to be added to the transmitted signal for the sake of satisfying the LED's forward current. After adding the DC bias, the transmitted signal having a power below $P_{Tx,min}$ and above $P_{Tx,max}$ will be clipped, which results in clipping noise [19]. Specifically, for ACO-OFDM, the discarded powers are $\varepsilon_{top} = P_{Tx,max} - P_{Tx,bias}$ and $\varepsilon_{bottom} = \max(P_{Tx,min} - P_{Tx,bias}, 0)$, respectively. Based on [20], if $\varepsilon_{bottom} = 0$, the bottom clipping will not impose any clipping noise because ACO-OFDM only employs odd (even) frequency subcarriers to convey information, while the clipping noise was shown to be confined to the even (odd) subcarriers. In this scenario, the SINR of the specific user k in the A-cell $\mathcal{C}_c$ can be written as:

$$\lambda_{c,k}^{clip} = \frac{\Lambda P_{Tx,opt}^2 \omega_c^2}{N_0 B + G_{DC} \sigma_{clip}^2 \omega_c^2 + \Lambda P_{Tx,opt}^2 \sum_{i \in S_I} (h_{i,k}^0 + h_{i,k}^1)^2}, \quad (5)$$

$$\Lambda = \frac{2\pi \gamma^2 K^2 G_{DC}}{G_B}, \quad (6)$$

where G_{DC} is the attenuation factor of the electrical signal power $P_{Tx,elec} = 2\pi P_{Tx,opt}^2$ due to the DC bias, which can be expressed as [19]:

$$G_{DC} = \frac{\sqrt{2\pi} P_{Tx,elec}}{\sqrt{2\pi} P_{Tx,elec} + 4\sqrt{P_{Tx,elec}} P_{Tx,bias} + 2\sqrt{2\pi} P_{Tx,bias}^2}. \quad (7)$$

Furthermore, K is the attenuation factor imposed by clipping, which is calculated as $Q(\xi_{top}) - Q(\xi_{bottom})$, where $Q(\cdot)$

represents the Gaussian Q function, $\xi_{top} = \varepsilon_{top}/\sqrt{P_{Tx,elec}}$ and $\xi_{bottom} = \varepsilon_{bottom}/\sqrt{P_{Tx,elec}}$. Furthermore, $G_B = 0.5$ represents the utilization of ACO-OFDM. Finally, the variance of clipping noise is represented by σ^2_{clip}, which can be written as:

$$\begin{aligned}\sigma^2_{clip} = P_{Tx,elec}\{&\varphi(\xi_{top})(2\xi_{bottom} - \xi_{top}) - \varphi(\xi_{bottom})\xi_{bottom} \\ &+ (\xi^2_{bottom} + 1)[Q(\xi_{bottom}) - Q(\xi_{top})] \\ &+ Q(\xi_{top})(\xi_{top} - \xi_{bottom})^2 - 2K^2\},\end{aligned} \tag{8}$$

where $\varphi(x) = \exp(-x^2/2)/2\pi$.

Based on Shannon's theorem, the system's achievable throughput using VT and ACO-OFDM is calculated according to:

$$C = \sum_c \sum_k \frac{B}{4} \log_2(1 + \lambda), \tag{9}$$

where λ denotes the SINR and can be calculated by either $\lambda_{c,k}$ or $\lambda^{clip}_{c,k}$.

III. Positioning

Again, a prerequisite of constructing A-Cells is the knowledge of the users' positions. Therefore, it is necessary to invoke indoor positioning algorithms. According to the survey by Liu *et al*. [13], several different indoor positioning techniques may be invoked, e.g. triangulation, scene analysis and proximity based solutions. In this paper, we will propose a novel hybrid positioning technique.

A. Triangulation

Triangulation is one of the classic positioning techniques that exploits the geometric properties of a triangle to estimate the users' locations. The Received-Signal-Strength (RSS) based triangulation aided positioning technique was applied in VLC environments in [13]. To elaborate, triangulation requires 3 reference APs with their coordinates denoted as (x_{n1}, y_{n1}), (x_{n2}, y_{n2}) and (x_{n3}, y_{n3}), respectively. Let the user's coordinate be (x_k, y_k). Then the system acquires the strongest RSS reading between the user and 3 different APs[1], which is denoted by $p^r_{k,ni} = P_{Tx,opt}(h^0_{k,ni} + h^1_{k,ni}), \quad i = 1, 2, 3$. According to Eq (1), the estimated distance $\tilde{d}_{k,ni}$ may be written as:

$$\tilde{d}_{k,ni} = \sqrt{\frac{A_r T_s(\psi) g(\psi) P_{Tx,opt} (H - h)^2}{\pi p^r_{k,ni}}}. \tag{10}$$

Given $\tilde{d}_{k,ni}$, the horizontal distance $\tilde{r}_{k,ni}$ can be calculated as:

$$\tilde{r}_{k,ni} = \sqrt{\tilde{d}^2_{k,ni} - (H - h)^2}. \tag{11}$$

Therefore, the linear system of equations used for estimating the user's coordinate $(\tilde{x}_k, \tilde{y}_k)$ is:

$$\begin{cases} (\tilde{x}_k - x_{n1})^2 + (\tilde{y}_k - y_{n1})^2 = \tilde{r}^2_{k,n1} \\ (\tilde{x}_k - x_{n2})^2 + (\tilde{y}_k - y_{n2})^2 = \tilde{r}^2_{k,n2} \\ (\tilde{x}_k - x_{n3})^2 + (\tilde{y}_k - y_{n3})^2 = \tilde{r}^2_{k,n3} \end{cases} \tag{12}$$

[1]This could be integrated into the cell search phase, where the APs transmit their sounding signals in an orthogonal way to the user. The user then measures the RSS and feeds it back to the system, which is assumed to be error free.

Eq (12) can be also streamlined into a matrix form as $\boldsymbol{AC} = \boldsymbol{B}$, where $\boldsymbol{C} = [\tilde{x}_k, \tilde{y}_k]^T$ and

$$\boldsymbol{A} = \begin{bmatrix} x_{n2} - x_{n1} & y_{n2} - y_{n1} \\ x_{n3} - x_{n1} & y_{n3} - y_{n1} \end{bmatrix}$$

$$\boldsymbol{B} = \frac{1}{2} \begin{bmatrix} (\tilde{r}^2_{k,n1} - \tilde{r}^2_{k,n2}) + (x^2_{n2} + y^2_{n2}) - (x^2_{n1} + y^2_{n1}) \\ (\tilde{r}^2_{k,n1} - \tilde{r}^2_{k,n3}) + (x^2_{n3} + y^2_{n3}) - (x^2_{n1} + y^2_{n1}) \end{bmatrix}.$$

Following least square estimation, the user coordinate can be estimated as $\boldsymbol{C} = (\boldsymbol{A}^T\boldsymbol{A})^{-1}\boldsymbol{A}^T\boldsymbol{B}$. Note that in order to estimate $(\tilde{x}_k, \tilde{y}_k)$, the matrix $\boldsymbol{A}$ should be full rank, implying that the 3 reference APs should not be in a single line.

A specific drawback of triangulation based positioning is that it is sensitive to the FOV. When the FOV is quite small, it is difficult to select 3 distinct APs, hence it is hard to satisfy the full-rank requirement. Another disadvantage is that the signal transmitted from the APs is subjected to reflections. When the reflections are strong, triangulation based positioning results into an inadequate performance.

B. Fingerprinting

To alleviate the potentially low accuracy of RSS-based triangulation aided positioning, scene analysis relying on probabilistic estimation could also be exploited, where RSS-based location fingerprinting is a commonly used technique. There are two basic fingerprinting steps: the off-line stage and on-line stage [13]. The off-line stage builds a useful reference position database for the scene, where the predefined reference coordinates and their RSS values are stored. The objective of the on-line stage is to estimate the user's location by comparing its RSS reading to that of the reference points in the database obtained from the off-line stage.

Let us assume that the specific room considered is divided into $(q \times t)$ small tiles. The RSS values of all tile centers are stored in the database and for the lth tile G_l, the RSS value stored is $p^r_l = \sum_{n=1}^N p^r_{l,n}$, where N is the number of APs. Let p^r_k be the aggregated RSS feedback of the kth user to be estimated, where $p^r_k = \sum_{n=1}^N p^r_{k,n}$ is obtained by superimposing all RSS values between the kth user and the N APs. Then tile G_i is preferred over G_j, if we have $P(G_i|p^r_k) > P(G_j|p^r_k)$, where $P(G_i|p^r_k)$ represents the probability of the kth user being located in G_i, given the aggregated RSS feedback of p^r_k. According to Bayes' theorem, we have the relationship of $P(G_i|p^r_k) = P(p^r_k|G_i)P(G_i)/P(p^r_k)$, where $P(p^r_k|G_i)$ represents the likelihood of the kth user having the aggregated RSS value of p^r_k, if the user was located in the tile G_i. Hence, given an equal *a prior* i probability of $P(G_i)$ $\forall i$, we have the relationship of $P(G_i|p^r_k) > P(G_j|p^r_k) \propto P(p^r_k|G_i) > P(p^r_k|G_j)$ for our decision concerning choosing G_i over G_j. Therefore, the decision rule obeys the Maximum Likelihood (ML) criteria. Naturally, a potential drawback of the RSS-based fingerprinting based position estimation on is the complexity of the full-search-based ML test, which relies on the completeness of the scene-specific database built during the off-line stage.

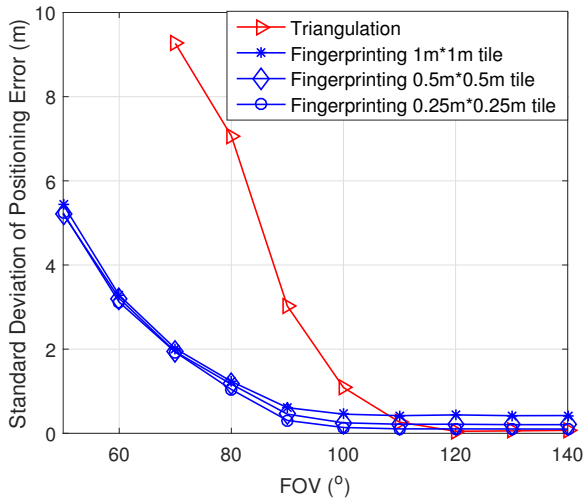

Fig. 2. Standard deviation of positioning error as a function of the FOV for both the triangulation based positioning and for the fingerprinting solution for a different tile size in the database.

C. Hybrid Positioning

Figure 2 shows the position error as a function of the FOV for both the triangulation based and for the fingerprinting aided positioning for different tile sizes in the database. In this figure, the position error is simply the Euclidean distance between the user's true position and estimated position. As we can see, fingerprinting has a much higher accuracy than triangulation based positioning. The tile size only has a modest effect on the accuracy. As discussed above, triangulation based positioning exhibits a low complexity and a beneficial scene independence, but it has low accuracy, when the FOV is small and when the users are located at the edge of the room, hence suffering from high reflections. By contrast, fingerprinting suffers from a higher complexity. Hence, we propose a hybrid positioning technique, combining the advantages of both to achieve a compelling balance between the complexity and accuracy.

More explicitly, there are two steps dedicated to realizing our hybrid positioning require. During the first step, it builds the fingerprinting database and applies triangulation based positioning to estimate all the users' positions. In the second step, each estimated position is classified into its corresponding tile of the database and returns the likelihood of being associated with that specific tile. If the likelihood is higher than a threshold, then the estimated position will be accepted and no more actions will be applied. Otherwise, the estimated position will be rejected and fingerprinting will be employed for re-positioning. Since triangulation based positioning is capable of estimating most positions under a reasonable FOV, only a few users have to use fingerprinting. Regardless of the number of tiles in the fingerprinting database, the total complexity is reduced compared to plain fingerprinting, especially when the number of users is high. In the mean time, the average positioning accuracy may be enhanced, when compared to the plain triangulation based positioning.

IV. Results

Let us now provide simulation results for characterizing the performance of the proposed hybrid positioning. The cell-radius threshold used in A-Cell construction is set to $4m$ and the likelihood threshold of the hybrid positioning is set to $10e^{-5}$. The fingerprinting database is built for $0.5m \times 0.5m$ tiles. In clipping scenario, the DC bias is $P_{Tx,bias} = 3.73mW$ and the linear dynamic range of a LED is set between $P_{Tx,min} = 5mW$ and $P_{Tx,max} = 50mW$. The remaining simulation parameters are included in the footnote[2]. We rely on two criteria for evaluating the performance of hybrid positioning, namely the positioning accuracy and the system's throughput.

A. Positioning Accuracy

When applying the hybrid positioning in our simulated room relying on a total of $8 \times 8 = 64$ APs, the logarithmic positioning error standard deviation evaluated across the entire room is shown in Figure 3(b). The corresponding normalized AP density is defined as the number of APs divided by the room area, which is $0.28/m^2$. Observe by comparing Figure 3(b) and Figure 3(a) that the positioning error recorded for our hybrid technique at the edge of the room is reduced to about $1m$ from about $10m$ seen for the triangulation based positioning. When we reduce the normalized AP density to $0.1/m^2$ by reducing the number of APs to $5 \times 5 = 25$, the triangulation based positioning and hybrid positioning may be compared in Figure 4. As expected, the general trend is that the accuracy is slightly degraded. Finally, when increasing the AP density to $0.87/m^2$, observe in Figure 5 that triangulation still has an estimation standard deviation of about $10m$ at the corner points, where it suffers from the strongest reflections and scattering [21]. By contrast, our hybrid positioning reduces it to around $1m$ in the corners and to about $0.1m$ or less in other positions.

Based on the above observations, we conclude that the proposed hybrid positioning is quite accurate right across the room considered, while dispensing with the full ML test of all users relied upon by the fingerprinting aided positioning.

B. System Throughput

The system's throughput can be calculated from Eq. (9), which is shown in hybrid positioning for different FOVs in the absence of clipping noise in Figure 6(a) and in the presence of clipping noise in Figure 6(b). When compared to triangulation based positioning, the hybrid positioning performs significantly better for low FOVs in both scenarios. Explicitly, when the FOV is lower than 70^o, triangulation based positioning fails, because the FOV is too low for adequately selecting the 3 different reference points required for positioning. On the other hand, the system's throughput achieved with the aid of hybrid positioning tends to be similar to that of fingerprinting,

[2]Semi-angle at half power (FWHM) ($\phi_{1/2}$) is 60°; O/E conversion efficiency (γ) is 0.53 (A/W); physical area of a PD's detector (A_r) is $1cm^2$; the gain of optical filter ($T_s(\psi)$) is 1; refraction index (n) is 1.5 and reflection efficiency (ρ) is 0.75.

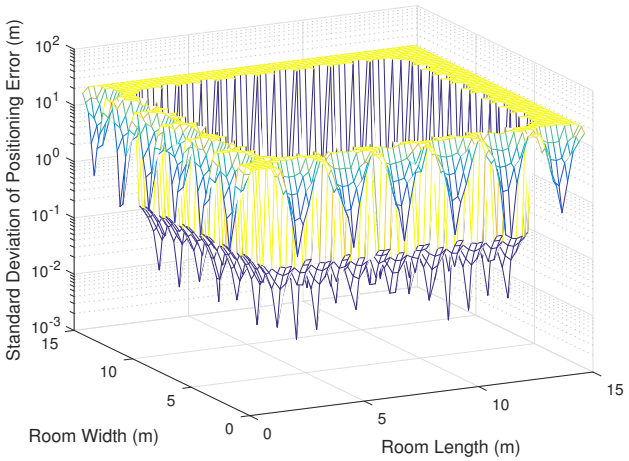

(a) Standard deviation of positioning error distribution using triangulation based positioning

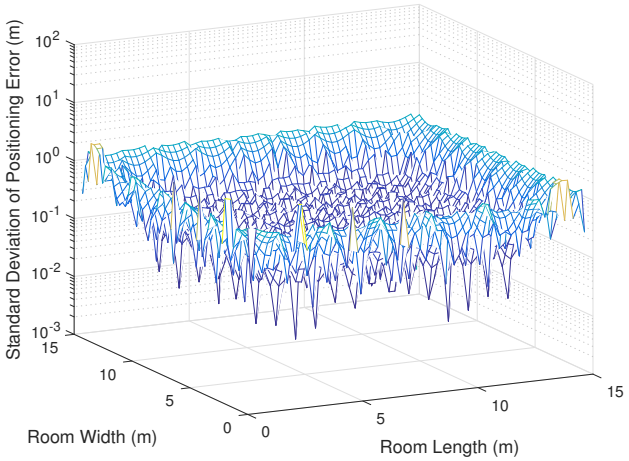

(b) Standard deviation of positioning error distribution using hybrid positioning

Fig. 3. Comparison of positioning accuracy between hybrid positioning and triangulation based positioning with AP density $0.28/m^2$.

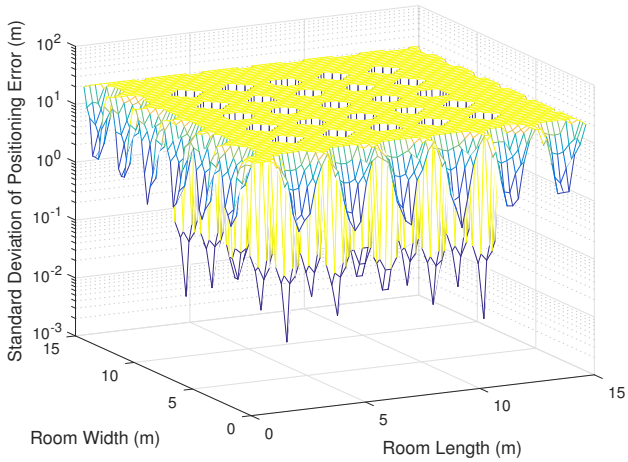

(a) Standard deviation of positioning error distribution using triangulation based positioning

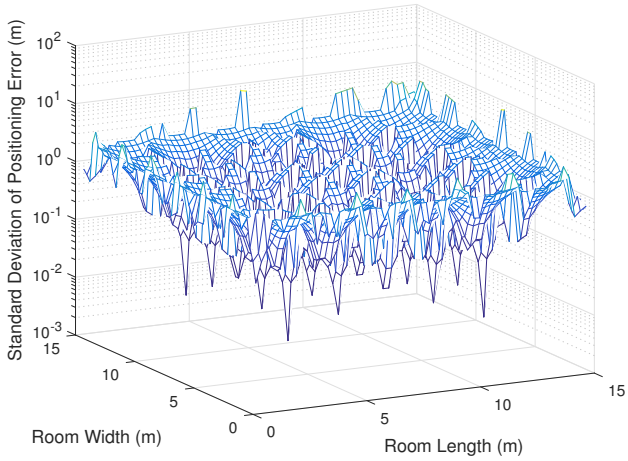

(b) Standard deviation of positioning error distribution using hybrid positioning

Fig. 4. Comparison of positioning accuracy between hybrid positioning and triangulation based positioning with AP density $0.1m^2$.

despite its lower complexity. Finally, both the fingerprinting and the hybrid positioning achieve a similar system throughput to that of perfect positioning, regardless of the specific level of performance considered.

Explicitly, Figure 7 shows the normalized throughput loss of all positioning techniques. The normalized throughput loss is calculated as the difference between the throughput associated with no clipping noise and having non-negligible clipping noise, which is further normalized with respect to the throughput associated with no clipping. It can be seen from this figure that when the FOV is high, the proposed hybrid positioning suffers from the lowest normalized throughput loss, approaching the throughput of the perfect positioning scenarios. On the other hand, fingerprinting based positioning suffers from the most grave normalized throughput loss. Finally, a common trend for all positioning techniques is that the normalized throughput loss becomes higher, when the FOV is lower. This is because when the FOV is low, the clipping noise effects tend to dominate, while the interference effects dominate for higher FOVs.

V. Conclusions

In this paper, we proposed a novel hybrid position technique for achieving the flexible construction of radius based A-Cells for indoor VLC under practical LED linearity constraints with clipping distortion and noise. More explicitly, by amalgamating the benefits of both triangulation and of fingerprinting, the proposed technique becomes capable of achieving a much higher positioning accuracy than triangulation at a lower complexity than fingerprinting, right across the entire room and for a range of FOVs. The resultant system throughput is also similar to that of perfect positioning. A substantial benefit of the proposed hybrid positioning technique is that it may be further combined with other positioning techniques for diverse applications.

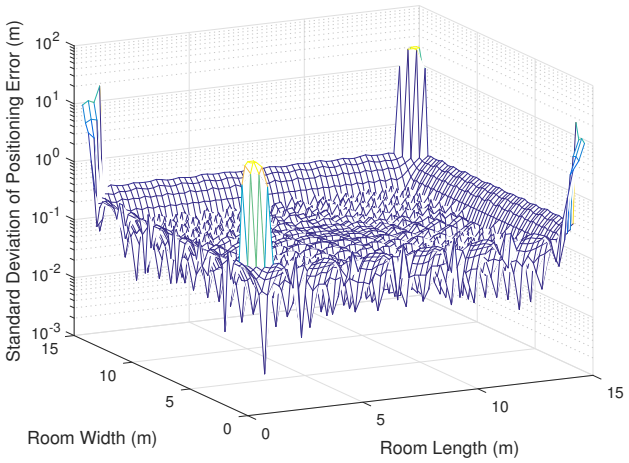

(a) Standard deviation of positioning error distribution using triangulation based positioning

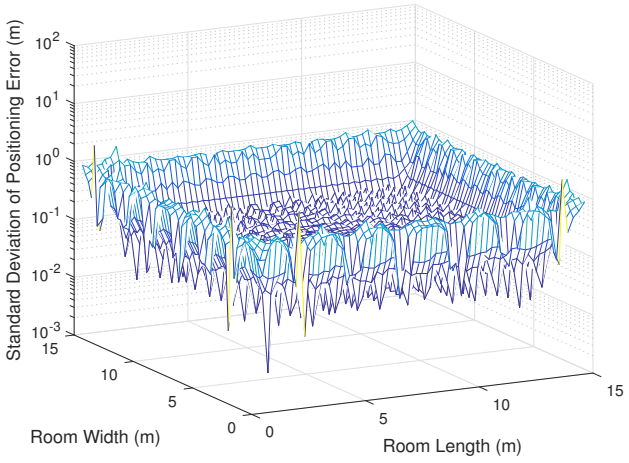

(b) Standard deviation of positioning error distribution using hybrid positioning

Fig. 5. Comparison of positioning accuracy between hybrid positioning and triangulation based positioning with AP density $0.87m^2$.

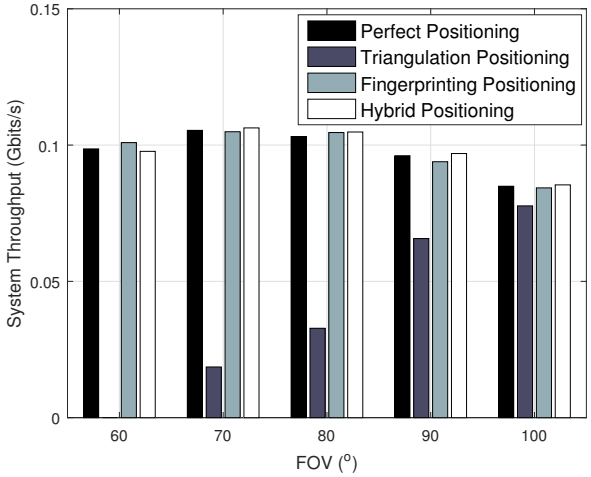

(a) System throughput under no clipping noise scenario

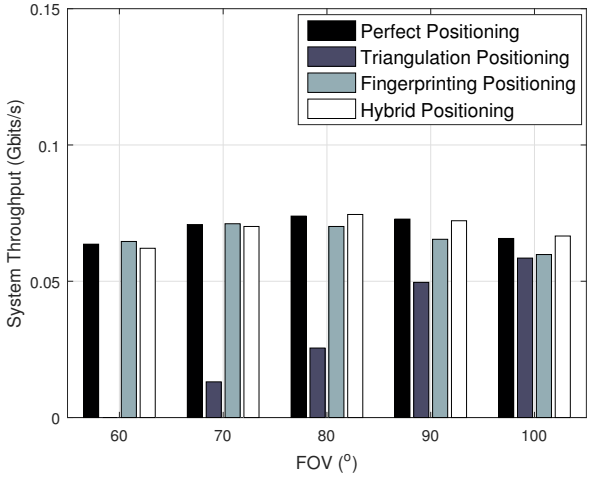

(b) System throughput under clipping noise scenario

Fig. 6. System throughput comparison between different positioning techniques v.s. the FOV.

REFERENCES

[1] L. Hanzo, H. Haas, S. Imre, D. O'brien, M. Rupp, and L. Gyongysi, "Wireless myths, realities, and futures: wireless 3G/4G to optical and quantum wireless," *IEEE Proceedings*, vol. 100, pp. 1853–1888, May 2012.

[2] W. Xu, M. Wu, H. Zhang, X. You, and C. Zhao, "ACO-OFDM-Specified recoverable upper clipped with efficient detection for optical wireless communication," *IEEE Photonics Journal*, vol. 6, no. 5, October 2014, Art. ID 7902617.

[3] C. Tang, M. Jiang, H. Shen, and C. Zhao, "Analysis and optimization of P-LDPC coded RGB-LED-based VLC system," *IEEE Photonics Journal*, vol. 7, no. 6, December 2015, Art.ID 7905213.

[4] S. Dissanayake and J. Armstrong, "Comparison of ACO-OFDM, DCO-OFDM and ADO-OFDM in IM/DD systems," *Journal of Lightwave Technology*, vol. 31, no. 7, pp. 1063–1072, April 2013.

[5] L. Wu, Z. Zhang, J. Dang, and H. Liu, "Adaptive modulation schemes for visible light communications," *Journal of Lightwave Technology*, vol. 33, no. 1, pp. 117–125, January 2015.

[6] F. Jin, R. Zhang, and L. Hanzo, "Resource allocation under delay-guarantee constraints for heterogeneous visible-light and RF femtocell," *IEEE Transactions on Wireless Communications*, vol. 14, no. 2, pp. 1020–1034, February 2015.

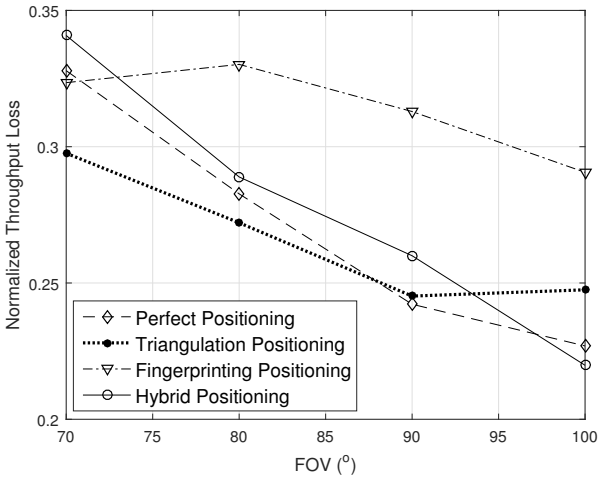

Fig. 7. Normalized throughput loss as a function of the FOV for different positioning techniques.

[7] X. Li, R. Zhang, and L. Hanzo, "Cooperative load balancing in hybrid visible light communications and WiFi," *IEEE Transactions on Communications*, vol. 63, no. 4, pp. 1319–1329, April 2015.

[8] K. Ying, H. Qian, R. Baxley, and S. Yao, "Joint optimization of precoder and equalizer in MIMO VLC systems," *IEEE Journal on Selected Areas in Communications*, vol. 33, no. 9, pp. 1949–1958, September 2015.

[9] A. Burton, H. L. Minh, Z. Ghassemlooy, E. Bentley, and C. Botella, "Experimental demonstration of 50-Mb/s visible light communication using 4*4 MIMO," *IEEE Photonics Technology Letters*, vol. 26, no. 9, pp. 945–948, May 2014.

[10] C.-L. I, C. Rowell, S. Han, Z. Xu, G. Li, and Z. Pan, "Toward green and soft: a 5G perspective," *IEEE Communications Magazine*, vol. 52, no. 2, pp. 66–73, February 2014.

[11] R. Zhang, J. Wang, Z. Wang, Z. Xu, C. Zhao, and L. Hanzo, "Visible light communications in heterogeneous networks: Paving the way for user-centric design," *IEEE Wireless Communications*, vol. 22, no. 2, pp. 8–16, April 2015.

[12] R. Zhang, H. Claussen, H. Haas, and L. Hanzo, "Energy efficient visible light communications relying on amourphous cells," *IEEE Journal on Selected Areas in Communications*, 2015, (Accepted).

[13] H. Liu, H. Darabi, P. Banerjee, and J. Liu, "Survey of wireless indoor positioning techniques and systems," *IEEE Transactions on Systems Man and Cybernetics*, vol. 37, no. 6, pp. 1067–1080, November 2007.

[14] W. Xu, J. Wang, H. Shen, H. Zhang, and X. You, "Indoor positioning for multiphotodiode device using visible-light communications," *IEEE Photonics Journal*, vol. 8, no. 1, February 2015, Art. ID 7900511.

[15] Y. Hou, S. Xiao, H. Zheng, and W. Hu, "Multiple access scheme based on block encoding time division multiplexing in an indoor positioning system using visible light," *IEEE/OSA Journal of Optical Communications and Networking*, vol. 7, no. 5, pp. 489–495, May 2015.

[16] M. Molina-Garcia, J. Calle-Sanchez, J. Alonso, A. Fernandez-Duran, and F. Barba, "Enhanced in-building fingerprinting positioning using femtocell networks," *Bell Labs Technical Journal*, vol. 18, no. 2, pp. 195–211, October 2013.

[17] T. Komine and M. Makagawa, "Fundamental analysis for visible-light communication system using LED lights," *IEEE Transactions on Consumer Electronics*, vol. 50, no. 1, pp. 100–107, February 2004.

[18] S. Dimitrov and H. Haas, "Information rate of OFDM-based optical wireless communication systems with nonlinear distortion," *Journal of Lightwave Technology*, vol. 31, no. 6, pp. 918–929, March 2013.

[19] S. Dimitrov, S. Sinanovic, and H. Haas, "Clipping noise in OFDM-based optical wireless communication systems," *IEEE Transactions on Communications*, vol. 60, no. 4, pp. 1072–1081, April 2012.

[20] J. Armstrong and B. Schmidt, "Comparison of asymmetrically clipped optical OFDM and DC-biased optical OFDM in AWGN," *IEEE Communications Letters*, vol. 12, no. 5, pp. 343–345, May 2008.

[21] W. Gu, M. A. Kashani, and M. Kavehrad, "Multipath reflections analysis on indoor visible light positioning system," *IEEE Physics and optics*, vol. 6, April 2015.

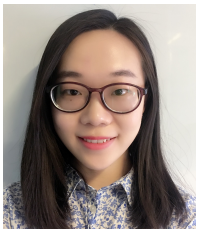

Simeng Feng received her B.Eng degree in Electronic Information Science and Technology from Ocean University of China and received her Master degree in Wireless Communications from University of Southampton, UK. Now, she is working towards her Ph.D. degree with Southampton Wireless, University of Southampton, UK. Her research interests include visible light communications, optical modulations, indoor positioning, amorphous cells, heterogeneous networks and energy efficiency.

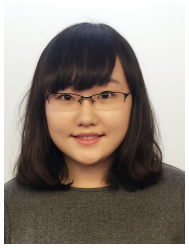

Xuan Li received her B.Eng degree (June 12) in Optical Information Science and Technology from Beijing Institute of Technology, China. She is currently working towards the PhD degree with Southampton Wireless, University of Southampton, UK. Her research interests include visible light communications, heterogeneous networks, resource allocation and video streaming.

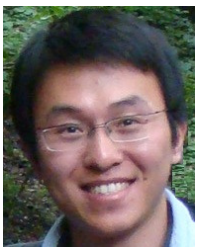

Rong Zhang (M'09) is an assistant professor in Southampton Wireless group within the school of ECS at University of Southampton (UoS). He received his PhD in wireless communications from UoS in 2009, where he was a research assistant during that period with Mobile Virtual Centre of Excellence, one of UK's largest industrial-academic partnership in ICT. During his post-doctoral period in ECS, he contributed as the UoS lead researcher on a number of international projects. After that, he took his industrial consulting leave for Huawei EU R&D as a System Algorithms Expert. He is also a guest researcher of the Centre in Next Generation Computational Modelling at UoS. He has a total of 70+ IEEE/OSA publications, including 40+ journals (20+ of which as first author). Owing to his outstanding academic achievements, he is the recipient of the prestigious Dean's Publication Award. He regularly serves as reviewer for IEEE/OSA journals and has been several times as TPC member/invited session chair of major conferences. He is a member of the IET, of the IEEE and is the recipient of joint funding of MVCE and EPSRC as well as the recipient of Worldwide University Network grant.

Ming Jiang (M'07-SM'13) received B.Eng. and M.Eng. degrees from South China University of Technology (SCUT), China, and Ph.D. degree from University of Southampton, UK, respectively, all in Electronic Engineering. Dr. Jiang has substantial international and industrial experience with Fortune 500 telecom companies. From 2006 to 2013, he had held key R&D and/or management positions at Samsung Electronics Research Institute (SERI), UK, Nortel's R&D Centre, China, and telecom equipment maker New Postcom, China, where he actively participated in numerous collaborative projects including European FP6 WINNER-II, FP7 DAVINCI, WiMAX/IEEE802.16m and LTE/LTE-A standardization, etc. across the EU, North America and Asia, on researching and designing novel algorithms, telecommunication standards as well as radio access and core network products. Since June 2013, he has been a Full Professor and Ph.D. Supervisor at Sun Yat-sen University, China, where he focuses on both scientific research and technology transfer with industrial partners. Dr. Jiang's research interest falls into next-generation wireless mobile communications, including MIMO, OFDM, VLC, D2D, HetNets, etc. He has co-authored or contributed to 5 Wiley books, 30 papers in prestigious international journals and conferences, 35 patents as well as 400+ LTE/LTE-A/WiMAX standardization contributions. Dr. Jiang is the recipient of several Chinese Council Awards in 2011, including Innovative Leading Talents, Outstanding Experts, and Top Overseas Scholars.

Lajos Hanzo (http://www-mobile.ecs.soton.ac.uk) FREng, FIEEE, FIET, Fellow of EURASIP, DSc received his degree in electronics in 1976 and his doctorate in 1983. In 2009 he was awarded an honorary doctorate by the Technical University of Budapest, while in 2015 by the University of Edinburgh. During his 40-year career in telecommunications he has held various research and academic posts in Hungary, Germany and the UK. Since 1986 he has been with the School of Electronics and Computer Science, University of Southampton, UK, where he holds the chair in telecommunications. He has successfully supervised 100+ PhD students, co-authored 20 John Wiley/IEEE Press books on mobile radio communications totalling in excess of 10 000 pages, published 1500+ research entries at IEEE Xplore, acted both as TPC and General Chair of IEEE conferences, presented keynote lectures and has been awarded a number of distinctions. Currently he is directing a 60-strong academic research team, working on a range of research projects in the field of wireless multimedia communications sponsored by industry, the Engineering and Physical Sciences Research Council (EPSRC) UK, the European Research Council's Advanced Fellow Grant and the Royal Society's Wolfson Research Merit Award. He is an enthusiastic supporter of industrial and academic liaison and he offers a range of industrial courses. He is also a Governor of the IEEE VTS. During 2008 - 2012 he was the Editor-in-Chief of the IEEE Press and a Chaired Professor also at Tsinghua University, Beijing. His research is funded by the European Research Council's Senior Research Fellow Grant. For further information on research in progress and associated publications please refer to http://www-mobile.ecs.soton.ac.uk Lajos has 24 000+ citations.